Journal of Materials Chemistry A

Insights into Dual-Functional Modification for Water Stability Enhancement of Mesoporous Zirconium Metal–Organic Frameworks

Journal:	*Journal of Materials Chemistry A*
Manuscript ID	TA-ART-05-2022-003851.R1
Article Type:	Paper
Date Submitted by the Author:	04-Aug-2022
Complete List of Authors:	Liu, Jian; Northwestern University, Chemistry; Argonne National Laboratory, Energy System Devision Anderson, Ryther; Colorado School of Mines Schmalbach, Kevin; University of Minnesota Twin Cities Sheridan, Thomas; Northwestern University Wang, Zhao; University of Minnesota Twin Cities Schweitzer, Neil; Northwestern University, Center for Catalysis and Surface Science; Argonne National Laboratory, Chemical Science and Engineering Division Stein, Andreas; University of Minnesota, Department of Chemistry Mara, Nathan; University of Minnesota Twin Cities Gomez-Gualdron, Diego; COLORADOSCHOOLOFMINES, Chemical and Biological Engineering Hupp, Joseph; Northwestern University, Department of Chemistry

SCHOLARONE™
Manuscripts

Journal of Materials Chemistry A

Insights into Dual-Functional Modification for Water Stability Enhancement of Mesoporous Zirconium Metal–Organic Frameworks

Received 00th January 20xx,
Accepted 00th January 20xx

DOI: 10.1039/x0xx00000x

Jian Liu,[*,a] Ryther Anderson,[b] Kevin M. Schmalbach,[c] Thomas R. Sheridan,[a] Zhao Wang,[d] Neil M. Schweitzer,[e] Andreas Stein,[d] Nathan A. Mara,[c] Diego Gomez-Gualdron,[b] and Joseph T. Hupp[*,a]

The stability of metal–organic frameworks (MOFs) in water affects their ability to function as chemical catalysts, their capacity as adsorbents for separations in water vapor presence, and their usefulness as recyclable water harvesters. Here, we have examined water stability of four node-modified variants of the mesoporous MOF, NU-1000, namely formate-, Acac-, TFacac-, and Facac-NU-1000, comparing these with node-accessible NU-1000. These NU-1000 variants present ligands grafted to NU-1000's hexa-Zr(IV)-oxy nodes by displacing terminal aqua and hydroxo ligands. Facac-NU-1000, containing the most hydrophobic ligands, showed the greatest water stability, being able to undergo at least 20 water adsorption/desorption cycles without loss of water uptake capacity. Computational studies revealed dual salutary functions of installed Facac ligands: 1) enhancement of framework mechanical stability due to electrostatic interactions; and 2) transformation and shielding of the otherwise highly hydrophilic nodes from H-bonding interactions with free water, presumably leading to weaker channel-stressing capillary forces during water evacuation – consistent with trends in free energies of dehydration across the NU-1000 variants. Water harvesting and hydrolysis of chemical warfare agent simulants were examined to gauge the functional consequences of modification and mechanical stabilization of NU-1000 by Facac ligands. The studies revealed a harvesting capacity of ~ 1.1 L of water vapor per gram of Facac-NU-1000 per sorption cycle. They also revealed retention of catalytic MOF activity following 20 water uptake and release cycles. This study provides insights into the basis for node-ligand-engendered stabilization of wide-channel MOFs against collapse during water removal.

Introduction

Metal–organic frameworks (MOFs) constitute a large class of porous crystalline materials which structures can be tuned by adjusting the inorganic node and organic linker components, leading to various materials with different topologies, pore sizes, and internal pore volumes.[1-9] Their stability in the presence of water, either in the form of liquid or vapor phase, is important for green syntheses of MOFs using water as the solvent[10-11] and for MOF applications in aqueous solutions or in variable-humidity environments.[12-13] MOFs can serve as heterogenous catalysts for hydrolytic detoxification of chemical warfare agents[14-16] and as electrocatalysts in water.[17-19] Water stability is also an important issue when considering MOFs as adsorbents for industrial gas separation and purification, as water vapor tends to competitively bind to open metal sites in MOF adsorbents and thereby inhibit binding of target chemicals.[20-21] For example, the co-existence of water vapor in post-combustion coal flue gas,[22] natural gas streams,[23] and the atmosphere[24] allows water to compete against CO_2, effectively poisoning open metal sites in MOFs. Therefore, evaluation of MOF performance in variable-humidity environments is important.

Yaghi and co-workers, as well as other researchers have demonstrated that MOFs can be used as recyclable water harvesters[25-30] if they have the following features: 1) unchanging water capacity across many adsorption-desorption cycles; 2) high water uptake; and 3) low regeneration temperature. A prerequisite for this application clearly is water stability of the selected MOFs. Hydrolytic stability and architectural stability are two critical factors to MOF water stability. The former can prevent the hydrolysis of the coordination bonds between nodes and linkers, while the latter allows the MOF to withstand the capillary force encountered during the water release process, thus preventing pore collapse. Reported approaches to enhancing MOF water stability include introducing highly connected nodes[25, 31] and employing strong and/or kinetically substitution-inert linker-node bonds.[27-28]

MOFs having microporosity usually show good water stability and low starting pressure for water uptake.[25, 32-33] However, due to their low pore volume, water uptake is not high. In contrast, MOFs containing mesopores typically display high water uptake in the first sorption cycle, but lose capacity in subsequent cycles.[34] One example is NU-1000,[35] which consists of $Zr_6(\mu_3\text{–}O)_4(\mu_3\text{–}OH)_4(H_2O)_4(OH)_4^{8+}$ nodes and tetratopic 1,3,6,8-tetrakis(*p*-benzoate)pyrene ($TBAPy^{4-}$)

[a.] *Department of Chemistry, Northwestern University, 2145 Sheridan Road, Evanston, Illinois 60208, United States.*
[b.] *Department of Chemical and Biological Engineering, Colorado School of Mines, Golden, Colorado 80401, United States.*
[c.] *Department of Chemical Engineering and Materials Science, University of Minnesota, Minneapolis, Minnesota 55455, United States.*
[d.] *Department of Chemistry, University of Minnesota, 207 Pleasant Street SE, Minneapolis, Minnesota 55455, United States.*
[e.] *Department of Chemical and Biological Engineering, Northwestern University, 2145 Sheridan Road, Evanston, Illinois 60208, United States.*
* Corresponding Authors. Emails: j-hupp@northwestern.edu, jian.liu@northwestern.edu.
Electronic Supplementary Information (ESI) available: [details of any supplementary information available should be included here]. See DOI: 10.1039/x0xx00000x

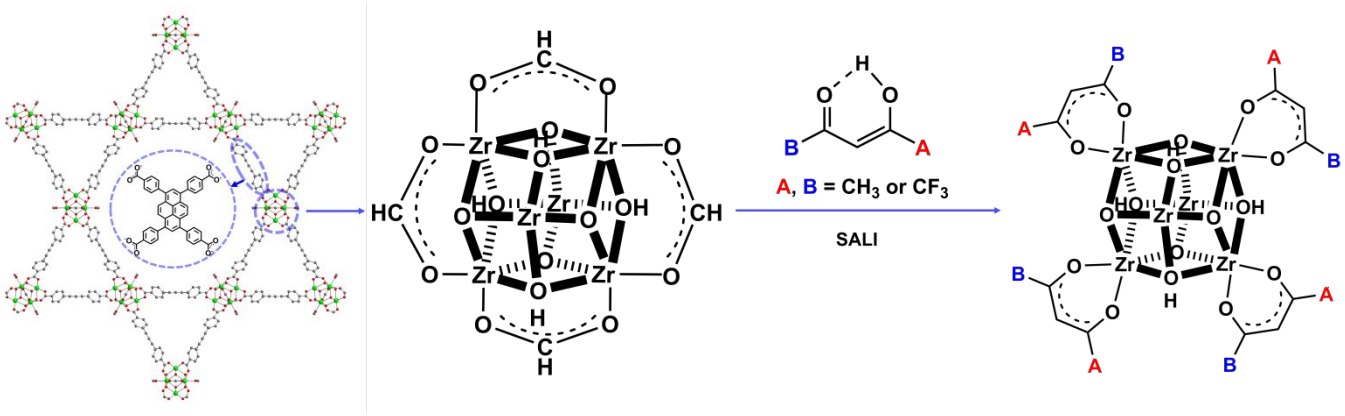

Figure 1. Schematic figure showing the preparation of target materials Acac-NU-1000, TFacac-NU-1000, and Facac-NU-1000 as well as their node structures. For clarity, 8 ligated $TBAPy^{4-}$ linkers are omitted from the node drawings. The bridging binding mode of formate ligands and the chelating binding mode of $Acac^-$/$TFacac^-$/$Facac^-$ ligands was obtained from single-crystal X-ray diffraction data in our previous studies.[14, 37]

linkers. Mondloch *et al.* hypothesized that capillary-force-driven channel collapse during the removal of water, rather than node-linker bond hydrolysis, is responsible for the structural failure.[36] Deria *et al.* showed that node-grafting of perfluoroalkane can impart stability toward water removal for NU-1000.[35] However, no studies have detailed the role(s) of installed ligands in enhancing MOF water stability.

Herein, we report on the extent to which compact, nonstructural ligands in modified NU-1000 contribute to water stability, in terms of both structural mechanical stability and their impact on capillary forces. Our previous studies have shown that the aqua/hydroxo ligands in NU-1000 can behave as displaceable site-holders for grafting non-structural ligands,[37-38] as reactive sites for immobilizing metal cations,[39-42] and as charge-compensating hydrogen bonding sites for noncovalently immobilizing halide ions.[14, 43] Each of three candidate non-structural ligands, acetylacetonate ($Acac^-$), 1,1,1-trifluoroacetylacetonate ($TFacac^-$), or hexafluoroacetylacetonate ($Facac^-$) was grafted, *via* SALI (solvent-assisted ligand incorporation), onto Zr_6-oxy nodes (**Figure 1**). The resulting materials are termed Acac-NU-1000, TFacac-NU-1000, and Facac-NU-1000. We reasoned that nonstructural chelating ligands could increase the energy cost for mechanical displacement of nodes by departing water, *i.e.*, by capillary forces, and thereby stabilize the framework against collapse. We further reasoned that these hydrophobic ligands could chemically transform and sterically shield the otherwise highly hydrophilic nodes from H-bonding interactions with mesopore-occupying water clusters, thereby diminishing capillary forces. As shown below, the modified materials indeed do exhibit enhanced stability against water evacuation. Comprehensive characterization combined with computational studies effectively explicate the basis for the observed enhanced stability.

Results and Discussion

Materials Synthesis and Characterization

A formate-containing version of NU-1000, termed NU-1000-F, can be synthesized using a modified reported method (see **Materials Synthesis** for details). ^{1}H-NMR spectroscopy (base digestion, peak at ~ 8.37 ppm) was used to quantify the formate ligands present (See **Figure S1**). Based on the linker-to-node ratio of 2:1, we observed 2.6 formate ligands present per Zr_6 node. (See **Table 1**). We have reported the installation of Facac and Acac onto Zr_6 nodes in NU-1000 *via* ALD, taking advantage of the high vapor pressure of HFacac and HAcac at room temperature. Single-crystal X-ray diffraction revealed that each ligand anion chelates to a single Zr ion, pointing into both hexagonal channels and pores perpendicular to the *c*-axis (**Figure 1**).[37] Solvent-assisted ligand incorporation (SALI), a similar process to ALD relying on acid–base chemistry, works similarly for installing ligands. The preparation details of ligand-modified MOFs are presented in the **Experimental** section. The number of $Acac^-$ ligands was quantified *via* ^{1}H spectroscopy (acid digestion), showing 4.0 per Zr_6 node in Acac-NU-1000, see **Figure S2 and Table 1**. A combination of ^{1}H and ^{19}F NMR spectroscopy was used to quantify the number of $Facac^-$ and $TFacac^-$ ligands incorporated using 1,3-bis(trifluoromethyl)-5-bromobenzene as an internal standard. The ligand loadings are 3.6 $Facac^-$ and 4.0 $TFacac^-$ per Zr_6 node for Facac-NU-1000 and TFacac-NU-1000, respectively, see **Figures S3-S6 and Table 1**. A formate-free version of NU-1000, termed NU-1000-FF, was also studied for comparison. The close-to-zero intensity of 8.37 ppm peak in the ^{1}H-NMR spectrum (**Figures S7**) and the absence of 2746 cm^{-1} in the DRIFT spectrum[44] (**Figure S9**) verified the removal of formate from NU-1000-FF and from other ligand-modified NU-1000 as well (**Figure S8 & S9, and Table 1**). The electronic withdrawing effect from the installed ligands was observed based on the O-H stretch shifting to lower wavenumbers in DRIFT spectra (**Figure S9**). The observed $-CF_3$ peak in the XPS C1s scan (**Figure S10**) confirmed the intact feature of $-CF_3$ ligands in TFacac- and Facac-NU-1000. Peak convolution on the XPS F1s scan (**Figure S10**) revealed the ligand loadings, which are 3.9 $Facac^-$ and 4.0 $TFacac^-$ per Zr_6 node, respectively, consistent with the NMR results. The crystallinity and porosity of the ligand-modified NU-1000 was confirmed by scanning electron microscopy (SEM) images (**Figure S11**), BET surface areas from N_2 isotherms (**Figure S12**), and pore-size distributions (**Figure S13**). Due to pore filling in the ligand-modified NU-1000 and contraction in NU-1000-FF, the pore volume decreases to ~ 1.35 and 1.18 cm^3/g for Acac/TFacac/Facac-NU-1000 and NU-1000-FF, respectively, compared with 1.57 cm^3/g for NU-1000-F (see **Table 1**).

This journal is © The Royal Society of Chemistry 20xx

Please do not adjust margins

Table 1. Loading of non-structural ligands, including formate, $Acac^-$, $TFacac^-$ and $Facac^-$, water uptake of 1st and 20th cycle at ~ P/P_0 = 0.9 measured at 287 K, and pore volumes derived from N_2 isotherms for five variants of NU-1000.

Sample Name	Formate (per Zr_6 node)	Ligands (per Zr_6 node)	Water Uptake 1st cycle (cm^3/g)(g/g)[a]	Water Uptake 20th cycle (cm^3/g)(g/g)	BET Surface Area (m^2/g)	Pore Volume (cm^3/g)
NU-1000-F	2.62	N/A	1540 (1.24)	490 (0.39)[b]	2190	1.57
NU-1000-FF	0.16	N/A	1200 (0.97)	490 (0.39)[b]	1850	1.18
Acac-NU-1000	0	4.00	1530 (1.23)	670 (0.54)[b]	1910	1.35
TFacac-NU-1000	0.04	3.98	1400 (1.1)	1180 (0.95)[c]	1920	1.33
Facac-NU-1000	0.02	3.55	1260 (1.0)	1250 (1.0)[c]	1970	1.36
NU-1000-F-Post	2.50	N/A	N/A	N/A	260	0.15
NU-1000-FF-Post	N/A	N/A	N/A	N/A	580	0.33
Acac-NU-1000-Post	N/A	0.50	N/A	N/A	740	0.34
TFacac-NU-1000-Post	N/A	3.80	N/A	N/A	1630	1.12
Facac-NU-1000-Post	N/A	3.41	N/A	N/A	1670	1.16

a, entries in the parentheses represent gravimetric uptakes with unit of g/g; b, recorded water uptake for the 2nd adsorption-desorption cycle; c, recorded water uptake for the 20th adsorption-desorption cycle.

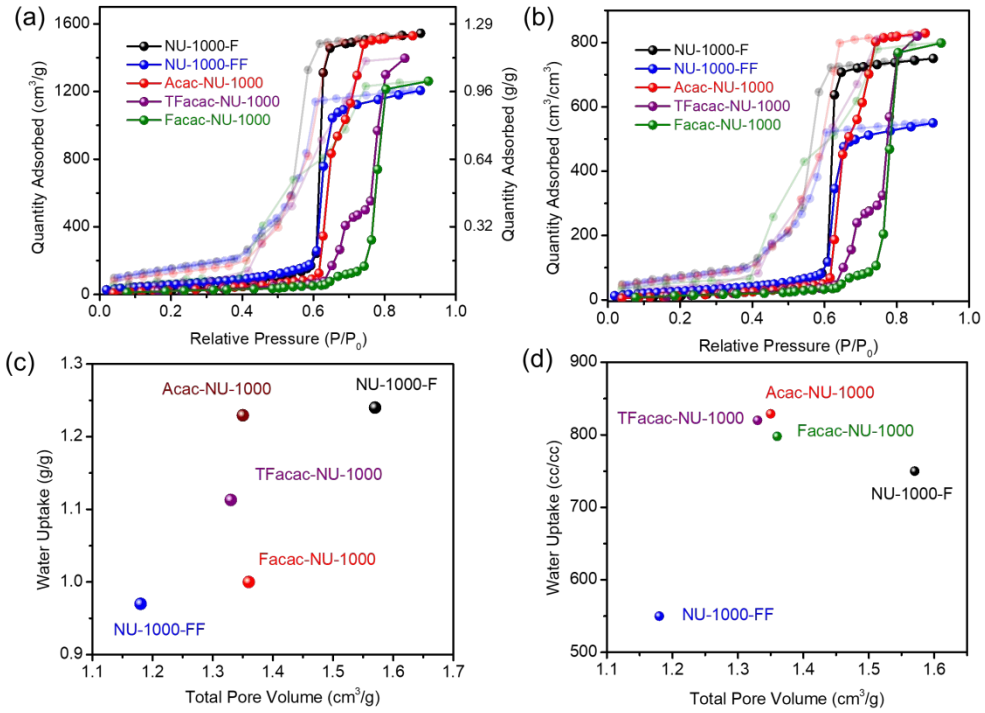

Figure 2. (a) Gravimetric and (b) volumetric water uptake of first-cycle water vapor isotherms for Acac-NU-1000, TFacac-NU-1000, Facac-NU-1000, NU-1000-F, and NU-1000-FF at 287K. The light lines stand for desorption curves. (c) and (d) Maximum water uptake of five variants of NU-1000 at P/P_0 = 0.9 as a function of total void volume obtained from N_2 isotherms.

Water Isotherm Measurements Showing Water Stability

The water isotherms were measured with relative pressure (P/P_0) between 0 and 0.9 at 14 °C (**Figure 2**). Water uptake behavior of NU-1000-F and NU-1000-FF was assessed under the same conditions for comparison (**Figures S14 & S15**). All samples were thermally treated under vacuum at 120 °C for 6 h before starting the measurements. The isotherm of NU-1000-FF (**Figure S15**) showed a steep uptake at ~ P/P_0 = 0.6, displaying type-V shape with a hysteresis loop at P/P_0 = 0.4–0.6 in water adsorption/desorption. This hysteresis loop is typically associated with pore filling with water vapor causing subsequent capillary condensation. The water uptake reached 1200 cm^3/g (0.97 g/g) at P/P_0 = 0.9 (**Table 1**). The formate-capped version, NU-1000-F, behaved similar to NU-1000-FF, both showing

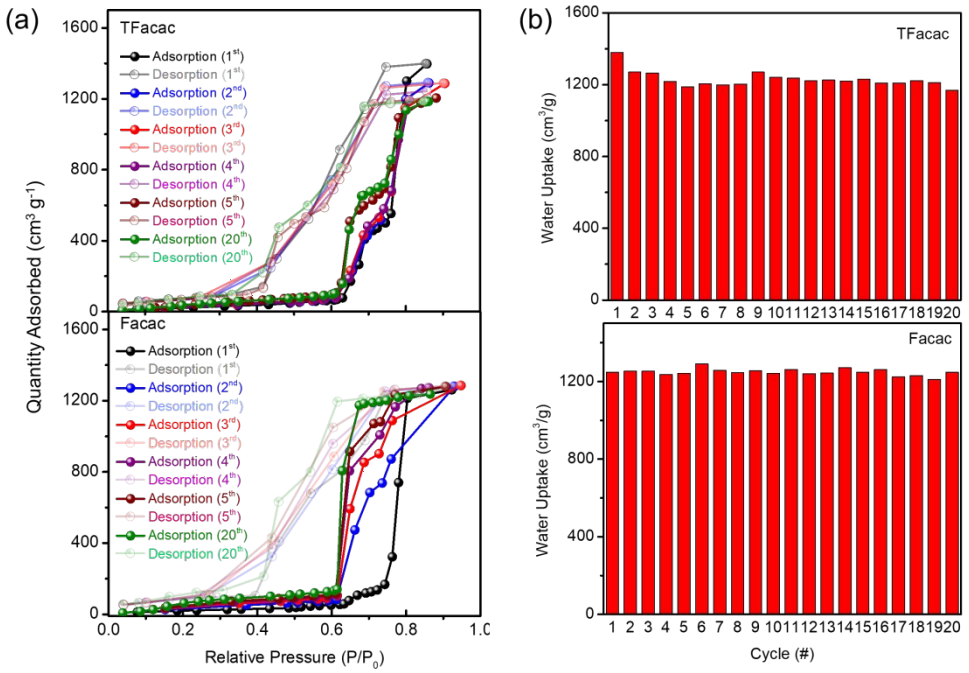

Figure 3. (a) Multiple-cycle water vapor isotherms of TFacac-NU-1000 and Facac-NU-1000. (b) The cycling test of TFacac-NU-1000 and Facac-NU-1000, showing 20 cycles water uptake with pressure swing between 20% RH (P/P_0 = 0.20) and 85% RH (P/P_0 = 0.85). Measurements were done at 287K.

approximate 70% capacity loss in the second water isotherm. The higher water uptake (1540 cm^3/g at P/P_0 = 0.9 in **Table 1**) in the first cycle presumably comes from the enlarged pore volume in NU-1000-F compared to NU-1000-FF (**Table 1**). N_2 isotherms on post-adsorption NU-1000-F/FF showed decreased surface areas and pore volumes (**Table 1**), indicating partial pore collapse.

The first-cycle water isotherms of ligand-modified NU-1000 are shown in **Figure 2a**. Similar to NU-1000-F/FF, only a small quantity of water is adsorbed in the low-pressure region, and the water uptake increases dramatically at P/P_0 = 0.6. In a change from NU-1000-F/FF, a second pressure step at higher P/P_0 (0.7–0.8) was observed, indicating a lower water affinity, and thus a higher required pressure for adsorption in these three materials. This observation is related to MOF pore hydrophobicity resulting from the installed ligands. Facac-NU-1000 also showed a steeper adsorption at higher relative pressure than Acac-NU-1000 and TFacac-NU-1000, presumably due to its higher hydrophobicity. The maximum uptake of Acac-, TFacac-, and Facac-NU-1000 was 1530 cm^3/g (1.2 g/g), 1400 cm^3/g (1.1 g/g), and 1260 cm^3/g (1.0 g/g), respectively, at P/P_0 = 0.90 and 287 K, see **Figure 2c**. These values are only slightly lower than the record uptake obtained from MIL-101-Cr (~ 1.3 g/g)[45] and Cr-soc-MOF-1 (~ 1.9 g/g).[27] For practical applications where space may be a limiting factor, the volumetric water uptake (cm^3/cm^3) is more meaningful than gravimetric water uptake (g/g), so we have also provided the volumetric uptakes in **Figures 2b & d**. These ligand-modified NU-1000 MOFs show higher water uptakes than either NU-1000-F or NU-1000-FF, at ~ 800 cm^3/cm^3. MIL-101-Cr and Cr-soc-MOF-1 show ~ 550 and ~ 910 cm^3/cm^3, respectively.

Multiple cycles of water isotherms were investigated to probe the water stability of the modified and unmodified MOFs, see **Figures 3a, and S14–S16**. After 5 adsorption–desorption cycles ($0<P/P_0<0.9$), another 14 cycles of two-point (P/P_0 = 0.20 and 0.85) measurements were performed followed by a 20th full adsorption–desorption isotherm. No thermal regeneration process was performed in between different cycles. The high water uptake of Acac-NU-1000 is not maintained across repeated cycles, losing ~ 60% of maximum water uptake in the 2nd cycle (**Figure S16**). TFacac- and Facac-NU-1000 showed excellent recyclability, as maximum water uptake in the 20th cycle was nearly identical to the 1st cycle (**Figure 3b**).

The porosity and ligand loadings of MOF samples were characterized after recording the 20th water isotherm. As shown in **Figures S17, S18, and Table 1**, the internal surface areas and pore volumes as determined from N_2 measurements were well retained for TFacac- and Facac-NU-1000 after twenty cycles of water adsorption-desorption isotherms. A dramatic decrease of surface area and pore volume, indicating pore collapse, was observed for NU-1000-F, NU-1000-FF, and Acac-NU-1000 after 2–3 water sorption cycles, see **Figure S17, S18, and Table 1** again. Residual ligands on MOFs after water isotherms were evaluated *via* NMR (both ^1H and ^{19}F) and XPS measurements. According to ^1H NMR in **Figures S19 and Table 1**, formate loading (2.5 per Zr_6) did not change after water isotherms with NU-1000-F. $Acac^-$ loading decreased to 0.5 per Zr_6, while the loadings of $TFacac^-$ and $Facac^-$ remained unchanged after 20 water sorption cycles (**Figures S20–S22**). The detachment of $Acac^-$ might be the result of good solubility and volatility of Hacac in water. Consistent with NMR spectra, the interpretation of XPS spectra revealed similar loadings of $TFacac^-$ and $Facac^-$ to those in as-synthesized MOFs, namely 3.9 and 3.3 per Zr_6 node, respectively (**Figures S23–S24**). SEM images combining with EDS line scans (**Figure S25**) showed that the five MOFs have similar crystallite morphologies and uniform fluorine distribution in TFacac- and Facac-NU-1000,

This journal is © The Royal Society of Chemistry 20xx

Please do not adjust margins

although pore collapse was observed in NU-1000-F/F and Acac-NU-1000 after water sorption.

Mechanical Testing

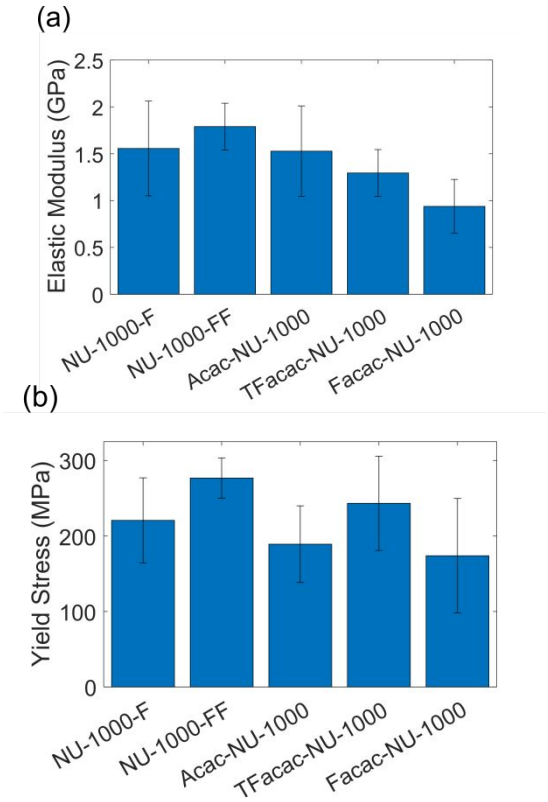

Figure 4. (a) Elastic modulus of the five NU-1000 variants as calculated from the stiffness of the loading curve and finite element simulations; (b) Yield stress of the five NU-1000 variants calculated from the failure load of the compression test and finite element simulations. Error bars for each indicate one standard deviation of four or more individual experiments.

One source of higher water stability of TFacac/Facac-NU-1000 might be enhanced mechanical stability. To test this hypothesis, we used a compression test followed by finite element simulation to obtain the elastic modulus and yield stress of all MOF materials. Using the initial slope of the loading curve (*i.e.*, the stiffness), the elastic modulus of each particle was calculated. All of the variants showed average elastic moduli in the range of about 1–1.75 GPa (**Figure 4a**). The error bars indicate one standard deviation; most of the variability is expected to be differences in contact conditions between the nanoindenter probe and the top of the particles. It is assumed that contact between the bottom of the indenter and the top of the particle is perfectly parallel. Deviation from perfect contact can possibly change from material to material, as the samples were all mounted on different SEM stubs. The yield stresses, as calculated from the failure load (the load at which the stiffness begins to drop from that seen in the purely elastic case), are all typically in the range of 175–275 MPa (**Figure 4b**), again with mostly overlapping error bars. Similar arguments about contact can be used regarding variation in yield stress. Considering the large standard deviation, these MOFs show more similar than different elastic modulus and yield stress when dry. Overall, it appears that these materials have similar mechanical properties which differ by an amount not detectable as measured here, which is in contrast to a previous study, where properties between phase-pure NU-1000 and NU-1000 with an NU-901 impurity phase varied by nearly an order of magnitude.[46]

Computational Investigation

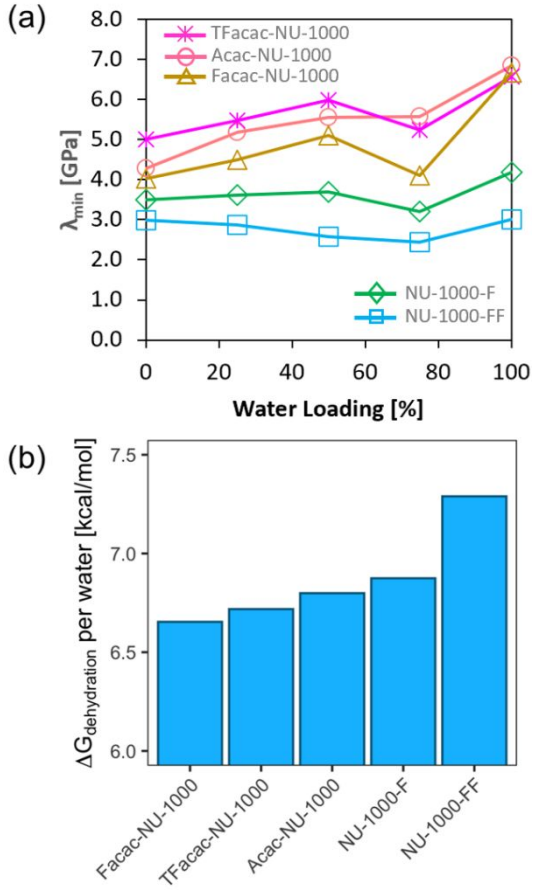

Figure 5. (a) Simulation-calculated smallest eigenvalue of the elastic tensor for the five variants of NU-1000 for different water loadings relative to maximum loading. Values are averages calculated from ten independent replicate simulations. (b) Free energies of dehydration (normalized by number of water molecules) $\Delta G_{dehydration}$ on five variants of NU-1000 calculated using finite differences thermodynamic integration (FDTI) method.

Given the difficulty in examining mechanical trends experimentally, computational studies were performed to investigate changes in mechanical properties due to ligand installation and interactions between water molecules and the NU-1000 variants during adsorption (desorption). Each version of the nodes for the variants was built according to our previously reported single crystal X-ray diffraction data,[14, 37] see **Figure S27**, and filled with water at various percent loadings relative to maximum adsorption capacity. Input structural files for the simulations are provided as **Supplementary Information**. Examination of the directional Young's moduli calculated for the MOFs at 0% water loading (**Figure S28-S29)** without and with intraframework electrostatic interactions reveals

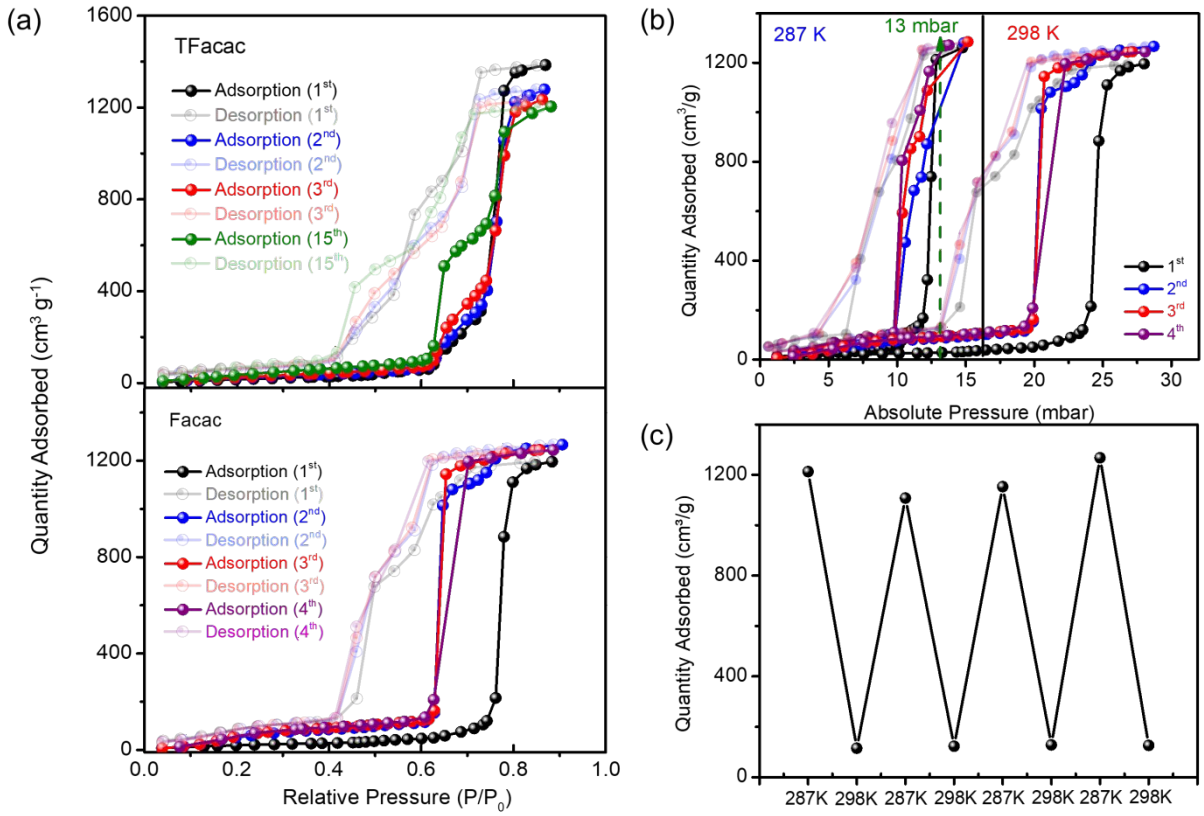

Figure 6. (a) Multiple-cycle water vapor isotherms of TFacac-NU-1000 and Facac-NU-1000 measured at 298K; (b) Water uptake vs. absolute pressure for four consecutive water cycles using Facac-NU-1000 performed at 287 K and 298 K; (c) Water uptake change demonstrating water adsorption and release as operation temperature changes between 287 K and 298 K using Facac-NU-1000. (The second and third data points at 287 K were estimated because no data point was collected at 13 mbar in the 2nd and 3rd water cycle.)

that changes in mechanical properties upon ligand installation are primarily due to electrostatic interactions (likely repulsions) rather than the bulkiness of $Acac^-$/$TFacac^-$/$Facac^-$ ligands.

While further quantitative evaluation of the directional Young's moduli (**Figure S30**) is appealing due to the potential tie to our compression experiments, Coudert and coworkers[47] advise examining the eigenvalues of the elastic tensor to evaluate mechanical stability trends. The latter quantities are presented in **Figures S31- S35** and **Table S1**, with trends for the smallest eigenvalue λ_{min} presented in **Figure 5a**. The eigenvalue λ_{min} is associated with the softest deformation mode, and the corresponding eigenvector indicates the direction of such mode. As water loading increases from 0% to 50%, there was at least a ca. 20% strengthening in the softest deformation mode in Acac/TFacac/Facac-NU-1000. However, in NU-1000-F the strengthening was significantly less pronounced (ca. 6%), while in NU-1000-FF the softest deformation mode became weaker (by ca. 14%).

We believe that these trends illustrate two competing effects: *i)* a strengthening "padding" effect due to water filling empty space, and *ii)* a weakening "pulling" effect due to strong interactions of water in partially filled pores "pulling" the pore walls of these structures inward to the pore centers. The weaker the framework is (*e.g.*, NU-1000-F and NU-1000-FF), the more apparent the pulling effect is. At 75% water-filling the pulling effect becomes apparent across all NU-1000 variants, with reductions between ca. 0% and ca. 20% occurring for λ_{min} with respect to the value at 50% water loading. We believe this effect is observed in all MOFs at 75% due to the collective pulling of a large number of water molecules, but with still sufficient empty pore space for the pore walls to be pulled into. Then, at 100% water filling (*i.e.*, without empty pore space), the padding effect takes over and all NU-1000 variants end up with a higher λ_{min} than that for 0% water loading. The padding effect is stronger in Acac/TFacac/Facac-NU-1000 with λ_{min}, with at least a ca. 31% increase in λ_{min} with respect to 0% water loading. For NU-1000-F and NU-1000-FF this increase is only ca. 20% and ca. 1%, respectively. Trends with water loadings aside, it is apparent from **Figure 5a** that NU-1000-FF and NU-1000-F are the least mechanically robust of the five MOFs studied. Hence installation of $Acac^-$/$TFacac^-$/$Facac^-$ ligands is shown to strengthen the framework.

In addition to framework strengthening, radial distribution functions (RDF) for the water oxygen-sp^3 carbon (O-C) pairs (**Figure S36**) and water oxygen-zirconium ion (O-Zr) pairs (**Figure S37**) revealed the changes in interactions between the water molecules and installed ligands, and the framework nodes, compared to unmodified NU-1000. The closest and farthest RDF peaks for O-C pairs occurred in $Acac^-$ and $Facac^-$ (**Figure S36**), respectively, which verified that the more hydrophobic effect from $Facac^-$ ligand behaving as a steric shield to prevent water getting closer to the

This journal is © The Royal Society of Chemistry 20xx

Please do not adjust margins

ligands. This effect has implications in shielding the Zr_6 nodes as well, with the RDFs and coordination plots (**Figure S37**) for O-Zr pairs showing water being able to associate more closely with the Zr_6 node in NU-1000-F/FF than in Acac/TFacac/Facac-NU-1000. Still, due to stronger hydrophobicity, Facac-NU-1000 appears better than Acac-NU-1000 in shielding the node from water.

The above presumably protects Facac-NU-1000 better from hydrolytic attack of node bonds with non-structural ligands (notice the post-adsorption loss of $Acac^-$ reported in **Table 1**). However, the shielding can also affect the interaction strength of water with the nodes, and thus presumably the capillary forces felt by the framework during water desorption. Accordingly, finite-difference thermodynamic integration (FDTI) was used to calculate the free energy of dehydration $\Delta G_{dehydration}$ (*i.e.*, the difference between the 100% water-loaded framework and the empty framework and isolated water molecules, **Figure 5b**).While in previous work[48] we have calculated MOF free energy as a measure of MOF thermodynamic stability, here $\Delta G_{dehydration}$ can be interpreted as the work required to extract all water from the framework to an ideal gas state, where a more positive $\Delta G_{dehydration}$ would be partly due to stronger water-framework interactions. Consistent with this picture, the poorest-shielding NU-1000-FF presents the highest $\Delta G_{dehydration,}$ while the strongest-shielding Facac-NU-1000 presents the lowest $\Delta G_{dehydration}$.

Focusing on the most mechanically robust variants, notice that while Acac-NU-1000 seems somewhat more mechanically robust than Facac-NU-1000, while the latter presumably offers better hydrolysis shielding. The smaller $\Delta G_{dehydration}$ contributes to Facac-NU-1000 experimentally displaying much better water cycling stability than Acac-NU-1000.

MOFs as Stable Water Harvesters

Since TFacac-NU-1000 and Facac-NU-1000 showed outstanding water stability and maintained high water uptake (~ 1 g/g) for at least 20 cycles, they are suitable for evaluation as water harvesting materials. Temperature-triggered capture and release of atmospheric water, during which water is adsorbed at night at low temperature (*e.g.*, 287 K) and released during the day at higher temperature (*e.g.*, 298 K), is a method to deliver fresh water using atmospheric thermal energy. Therefore, we measured the water capture using TFacac- and Facac-NU-1000 at 298 K, see **Figure 6a**. Compared with the maximum uptake at 287 K in **Figure 3a**, the water uptake at $P/P_0 = 0.90$ is essentially identical, with values of 1385 and 1196 cm^3/g for TFacac- and Facac-NU-1000, respectively. The water stability of the frameworks and the steep step at $P/P_0 = 0.7–0.8$ were also retained (**Figures 4a & S17**). For water vapor under constant absolute pressure, relative humidity during the night is high due to the low temperature and MOF materials can be used to adsorb water. When the temperature rises during the day, the relative humidity is low and the water will be released. Water uptake vs. absolute pressure using Facac-NU-1000 at each of two temperatures (287 K and 298 K) is shown in **Figure 6b**. At an absolute pressure of 13 mbar (green arrow in **Figure 6b**), the relative humidity (RH) will be 80% at 287 K, decreasing to 40% at 298 K, while the water adsorption capacity at 287 K is ~ 1200 cm^3/g and the desorption residual at 298 K is ~ 120 cm^3/g. The RH and uptake capacity did not change for at least four cycles. By changing temperature between 287 K and 298 K at 13 mbar, the water uptake and release process can be mimicked, see **Figure 6c**. In principle, this MOF would be able to providing ~ 1.1 L of condensable water vapor per gram of MOF per day/night cycle (thermal cycle), equivalent to ~1 g of liquid water per cycle. Arguably more relevant for practical applications is the volumetric yield of ~0.7 g (0.7 mL) of liquid water per cm^3 of MOF per thermal cycle (where, for simplicity, we have neglected MOF crystallite packing inefficiencies and treated the material as if it is a perfect monolith).

MOFs as Environment-stable (Storage-stable) Catalysts for Detoxification of Chemical Warfare Agent Simulants

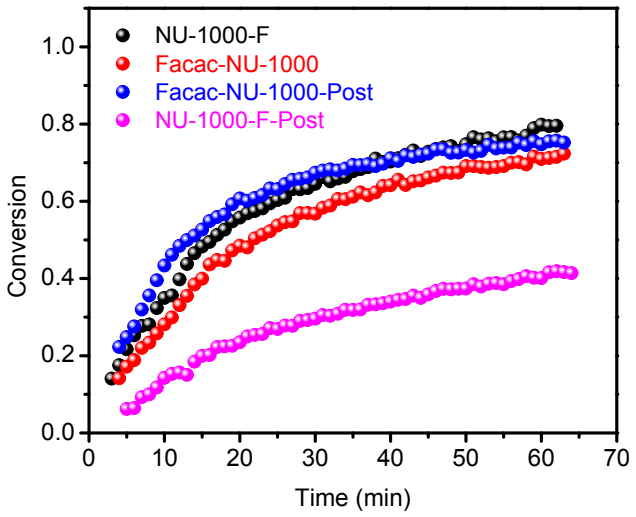

Figure 7. Hydrolysis profile of DMNP with Facac-NU-1000 before and after water adsorption-desorption isotherms compared to NU-1000-F.

NU-1000 has been extensively investigated as a catalyst for hydrolytic detoxification of G-type, organophosphate-based nerve agents and for similar hydrolysis of agent simulants, such as dimethyl 4-nitrophenylphosphate (DMNP).[49-50] We anticipated that the enhanced water stability of Facac-NU-1000 would protect the MOF from collapse during storage and/or transport in variable-humidity environments and thereby facilitate retention of catalytic competency. As a proof of concept, we investigated DMNP hydrolysis using Facac-NU-1000 and NU-1000-F after three water adsorption-desorption cycles and compared their performance with as-prepared MOFs. The catalysts were soaked in 0.4 M *N*-ethylmorpholine aqueous solution overnight to remove the capping ligands (*i.e.*, formate and Facac) prior to hydrolysis experiments. (The high solution pH (~10.5) in the presence of *N*-ethylmorpholine facilitates capping ligand removal.) As shown in **Figure 7**, Facac-NU-1000 after water sorption showed a reaction progress curve that is only moderately shifted from that obtained without prior water sorption & desorption (*i.e.*, initial hydrolysis reaction half-lives of 22 and 13 mins, respectively), as well as that obtained with as-synthesized NU-1000-F (*i.e.*, initial half-life of 16 mins). For a sample of NU-1000-F, termed NU-1000-F-Post, that was evaluated only after being first subjected to one water sorption-desorption cycle (one isotherm measurement), reaction progress was considerably slower – only ~ 40% in an hour. We attribute the diminished catalytic activity to pore

collapse, that, in turn, either slows DMNP diffusion to such a degree that reactant transport becomes rate-limiting, or else blocks DMNP access to candidate catalyst active-sites (or both). Initial reaction rates, determined from data collected in the first 5 mins were found to be 1.1, 0.3, 0.9, and 1.3 µmol/min for NU-1000-F, NU-1000-F-Post, Facac-NU-1000, and Facac-NU-1000-Post, respectively. The debilitating consequences of pore-collapse upon the hydrolytic catalytic activity NU-1000-F underscore the desirability of inhibiting collapse for eventual applications of catalysts to reactions involving aerosolized chemical threats, where water for hydrolysis is recruited from the external atmosphere, as well as for applications in the condensed phase where samples have been pre-exposed to variable humidity conditions. Facac modification would appear to be a solution to both problems. Alternatively, careful selection of MOFs featuring smaller pores would be desirable, as these are typically less susceptible than large-pore MOFs to pore collapse by water evacuation. Finally, the ability Facac-NU-1000 to recruit unusually large amounts of water from the external atmosphere would appear to be a considerable advantage for the above-mentioned applications involving reactants in aerosol or volatile-vapor form.

Conclusions

Five variants of NU-1000 (NU-1000-FF/F and Acac/TFacac/Facac-NU-1000) were prepared, and their capacity for water sorption was examined. We find that the maximum adsorbed water quantity in the first cycle varies in proportion to internal pore volume. The hydrophobicity of the installed non-structural ligands influences the onset point (*i.e.*, relative partial pressure) for steep uptake of water, with the onset point shifting to higher partial pressure as pore hydrophobicity increases. For Facac-NU-1000, the steep uptake occurs at $P/P_0 \sim 0.7$). Water uptake capacities for NU-1000-F, NU-1000-FF, and Acac-NU-1000 decrease markedly after only one sorption/desorprtion cycle, while for Facac-NU-1000 and TFacac-NU-1000 uptake capacities for the 20th cycle are nearly the same as for the 1st cycle. These observations point to hydrophobicity of node-modifying, nonstructural ligands behave as a salient property for engendering MOF stability against pore collapse during water evacuation.

Experimental mechanical testing did not reveal significant differences in elastic moduli (Young's moduli) and yield stresses across variants, albeit with unavoidably large measurement uncertainties potentially obscuring trends in these quantities. Computational studies were used to clarify mechanical stability trends across variants. Changes in mechanical properties upon ligand installation were to be due to electrostatic interactions rather than sterics. All the NU-1000 variants (which feature the low-symmetry **csq** topology) presented decidedly anisotropic mechanical properties. Comparisons of the elastic tensor eigenvalue associated with the softest deformation mode (λ_{min}) indicated two groupings: frameworks containing nodes modified by Acac$^-$, TFacac$^-$, or Facac$^-$ ligands are characterized by comparatively larger λ_{min} values, while NU-1000-FF and NU-1000-F are characterized by low λ_{min} values. The bimodal grouping is evident both with and without water in the MOF pores. Within the most mechanically robust grouping, Facac-NU-1000 presented better node shielding than Acac-NU-1000 according to radial distribution function analysis, presumably due to higher ligand hydrophobicity. Shielding protects otherwise hydrophilic Zr_6 nodes from undesirable hydrogen bonding to evacuable, pore-sited water clusters. Additionally, calculations of free energy of dehydration $\Delta G_{dehydration}$ (as a proxy for capillary forces felt upon water evacuation) also suggest less pronounced water pulling during evacuation on Facac-NU-1000 than in Acac-NU-1000, consistent with experimental water stability trends during water sorption cycling.

Experimental evaluation of Facac-NU-1000 as a candidate water harvester at fixed absolute vapor pressure (13 mbar) established that nearly all the water adsorbed at 287 K can be released thermally and spontaneously at 298 K. This material is capable of capturing and then releasing ~ 1,100 cm^{-3} of water vapor per gram of MOF per thermal cycle. DMNP hydrolysis was investigated using Facac-NU-1000 and NU-1000-F after water adsorption-desorption cycles and results were compared with those of as-prepared MOFs. The initial rate of NU-1000-F post water sorption decreased to about a quarter of its value before water sorption measurement. We attribute the deleterious rate effect, accompanying pore collapse, either to slowing of DMNP diffusion to the extent that mass transport becomes rate-determining or to blockage of access potential catalytic sites, or both. The combined results illustrate and explicate a potentially transferrable strategy for rendering mesoporous MOFs water stable. Enhancing framework mechanical stability while decreasing the capillary force exerted during water desorption, allows for the synthesis of mesoporous MOFs offering functionally advantageous water stability.

Conflicts of interest

The authors declare no competing financial interest.

Acknowledgements

J. T. H. gratefully acknowledges support from the National Science Foundation via grant number DMREF-2119433 and from Northwestern University. For studies of catalytic hydrolysis he gratefully acknowledges the Defense Threat Reduction Agency *via* grant number HDTRA1-19-1-0010. D. A. G.-G. gratefully acknowledges funding from the NSF through CAREER Award CBET-1846707. T. R. S. gratefully acknowledges support from a National Defense Science and Engineering Graduate Fellowship. Mechanical testing described in this work was primarily supported by the MRSEC Program of the National Science Foundation under Award Number DMR-2011401. Parts of this work were carried out in the Characterization Facility, University of Minnesota, which receives partial support from NSF through the MRSEC program. K. M. S. and N. A. M. acknowledge the Minnesota Supercomputing Institute (MSI) at the University of Minnesota for providing resources that contributed to the research results reported within this paper. This work made use of the J. B. Cohen X-ray Diffraction Facility supported by the MRSEC program of the National Science Foundation (DMR-1121262) at the Materials Research Center of Northwestern University. This work made use of the EPIC and Keck-II facilities of the NUANCE Center at Northwestern University, which has received support from the Soft and Hybrid Nanotechnology Experimental (SHyNE) Resource (NSF NNCI-1542205); the MRSEC program (NSF DMR-1121262) at the Materials Research Center; the International

 This journal is © The Royal Society of Chemistry 20xx

Please do not adjust margins

Institute for Nanotechnology (IIN); the Keck Foundation; and the State of Illinois, through the IIN. The REACT Facility of the Northwestern University Center for Catalysis and Surface Science is supported by a grant from the DOE (DE-SC0001329).

Notes and references

1. S. Horike, S. Shimomura, S. Kitagawa, *Nat. Chem.* 2009, **1**, 695-704.
2. D. Alezi, I. Spanopoulos, C. Tsangarakis, A. Shkurenko, K. Adil, Y. Belmabkhout, M. O'Keeffe, M. Eddaoudi, R. N. Trikalitis, *J. Am. Chem. Soc.* 2016, **138**, 12767-12770.
3. O. M. Yaghi, *J. Am. Chem. Soc.* 2016, **138**, 15507-15509.
4. C. Wang, D. Liu, W. Lin, *J. Am. Chem. Soc.* 2013, **135**, 13222-13234.
5. H. C. Zhou, J. R. Long, O. M. Yaghi, *Chem. Rev.* 2012, **112**, 673-674.
6. J. H. Cavka, S. Jakobsen, U. Olsbye, N. Guillou, C. Lamberti, S. Bordiga, K. P. Lillerud, *J. Am. Chem. Soc.* 2008, **130**, 13850.
7. T. C. Wang, N. A. Vermeulen, I. S. Kim, A. B. Martinson, J. F. Stoddart, J. T. Hupp, O. K. Farha, *Nat. Protoc.* 2016, **11**, 149-162.
8. Z. Lu, R. Wang, Y. Liao, O. K. Farha, W. Bi, T. R. Sheridan, K. Zhang, J. Duan, J. Liu, J. T. Hupp, *Chem Commun* 2021, **57**, 3571-3574.
9. J. E. Mondloch, W. Bury, D. Fairen-Jimenez, S. Kwon, E. J. DeMarco, M. H. Weston, A. A. Sarjeant, S. T. Nguyen, P. C. Stair, R. Q. Snurr, O. K. Farha, J. T. Hupp, *J. Am. Chem. Soc.* 2013, **135**, 10294-10297.
10. M. Sánchez-Sánchez, N. Getachew, K. Díaz, M. Díaz-García, Y. Chebude, I. Díaz, *Green Chem.* 2015, **17**, 1500-1509.
11. Z. Chen, X. Wang, T. Islamoglu, O. K. Farha, *Inorganics* 2019, **7**.
12. M. Taddei, J. A. Bokhoven, M. Ranocchiari, *Inorg. Chem.* 2020, **59**, 7860-7868.
13. G. Weber, I. Bezverkhyy, J. P. Bellat, A. Ballandras, G. Ortiz, G. Chaplais, J. Patarin, F. X. Coudert, A. H. Fuchs, A. Boutin, *Microporous and Mesoporous Mater.* 2016, **222**, 145-152.
14. Z. Lu, J. Liu, X. Zhang, Y. Liao, R. Wang, K. Zhang, J. Lyu, O. K. Farha, J. T. Hupp, *J. Am. Chem. Soc.* 2020, **142**, 21110-21121.
15. J. Liu, L. R. Redfern, Y. Liao, T. Islamoglu, A. Atilgan, O. K. Farha, J. T. Hupp, *ACS Appl. Mater. Interfaces* 2019, **11**, 47822-47829.
16. Y. Liao, T. Sheridan, J. Liu, O. K. Farha, J. T. Hupp, *ACS Appl. Mater. Interfaces* 2021, **13**, 30565-30575.
17. S. Mukhopadhyay, O. Basu, R. Nasani, S. K. Das, *Chem. Commun.* 2020, **56**, 11735-11748.
18. Z. Xue, K. Liu, Q. Liu, Y. Li, M. Li, C. Y. Su, N. Ogiwara, H. Kobayashi, H. Kitagawa, M. Liu, G. Li, *Nat. Commun.* 2019, **10**, 5048.
19. P. Q. Liao, J. Q. Shen, J. P. Zhang, *Coord. Chem. Rev.* 2018, **373**, 22-48.
20. J. Liu, Y. Wang, A. I. Benin, P. Jakubczak, R. R. Willis, M. D. LeVan, *Langmuir* 2010, **26**, 14301-14307.
21. M. I. Hossain, J. D. Cunningham, T. M. Becker, B. E. Grabicka, K. S. Walton, B. D. Rabideau, T. G. Glover, *Chem. Eng. Sci.* 2019, **203**, 346-357.
22. O. T. Qazvini,S. G. Telfer, *ACS Appl. Mater. Interfaces* 2021, **13**, 12141-12148.
23. I. Erucar, S. Keskin, *Ind. Eng. Chem. Res.* 2020, **59**, 3141-3152.
24. E. S. Sanz-Perez, C. R. Murdock, S. A. Didas, C. W. Jones, *Chem. Rev.* 2016, **116**, 11840-11876.
25. H. Furukawa, F. Gandara, Y. B. Zhang, J. Jiang, W. L. Queen, M. R. Hudson, O. M. Yaghi, *J. Am. Chem. Soc.* 2014, **136**, 4369-4381.
26. A. J. Rieth, S. Yang, E. N. Wang, M. Dinca, *ACS Cent. Sci.* 2017, **3**, 668-672.
27. S. M. Towsif Abtab, D. Alezi, P. M. Bhatt, A. Shkurenko, Y. Belmabkhout, H. Aggarwal, Ł. J. Weseliński, N. Alsadun, U. Samin, M. N. Hedhili, M. Eddaoudi, *Chem* 2018, **4**, 94-105.
28. Z. Chen, P. Li, X. Zhang, P. Li, M. C. Wasson, T. Islamoglu, J. F. Stoddart, O. K. Farha, *J. Am. Chem. Soc.* 2019, **141**, 2900-2905.
29. W. Xu, O. M. Yaghi, *ACS Cent. Sci.* 2020, **6**, 1348-1354.
30. A. J. Rieth, A. M. Wright, G. Skorupskii, J. L. Mancuso, C. H. Hendon, M. Dinca, *J. Am. Chem. Soc.* 2019, **141**, 13858-13866.
31. F. Fathieh, M. J. Kalmutzki, E. A. Kapustin, P. J. Waller, J. Yang, O. Yaghi, *Sci. Adv.*, 2018, **4**: eaat3198.
32. R. G. AbdulHalim, P. M. Bhatt, Y. Belmabkhout, A. Shkurenko, K. Adil, L. J. Barbour, M. Eddaoudi, *J. Am. Chem. Soc.* 2017, **139**, 10715-10722.
33. S. Wang, J. S. Lee, M. Wahiduzzaman, J. Park, M. Muschi, C. Martineau-Corcos, A. Tissot, K. H. Cho, J. Marrot, W. Shepard, G. Maurin, J. S. Chang, C. Serre, *Nat. Energy* 2018, **3**, 985-993.
34. S. Oien-Odegaard, B. Bouchevreau, K. Hylland, L. Wu, R. Blom, C. Grande, U. Olsbye, M. Tilset, K. P. Lillerud, *Inorg. Chem.* 2016, **55**, 1986-1991.
35. P. Deria, Y. G. Chung, R. Q. Snurr, J. T. Hupp, O. K. Farha, *Chem. Sci.* 2015, **6**, 5172-5176.
36. J. E. Mondloch, M. J. Katz, N. Planas, D. Semrouni, L. Gagliardi, J. T. Hupp, O. K. Farha, *Chem. Commun.* 2014, **50**, 8944-8946.
37. J. Liu, J. Ye, Z. Li, K. I. Otake, Y. Liao, A. W. Peters, H. Noh, D. G. Truhlar, L. Gagliardi, C. J. Cramer, O. K. Farha, J. T. Hupp, *J. Am. Chem. Soc.* 2018, **140**, 11174-11178.
38. J. Liu, Z. Li, X. Zhang, K. I. Otake, L. Zhang, A. W. Peters, M. J. Young, N. M. Bedford,S. P. Letourneau, D. J. Mandia, J. W. Elam, O. K. Farha, J. T. Hupp, *ACS Catal.* 2019, **9**, 3198-3207.
39. X. Wang, X. Zhang, R. Pandharkar, J. Lyu, D. Ray, Y. Yang, S. Kato, J. Liu, M. C. Wasson, T. Islamoglu, Z. Li, J. T. Hupp, C. J. Cramer, L. Gagliardi, O. K. Farha, *ACS Catal.* 2020, **10**, 8995-9005.
40. T. A. Goetjen, X. Zhang, J. Liu, J. T. Hupp, O. K. Farha, *ACS Sustain. Chem. Eng.* 2019, **7**, 2553-2557.
41. Z. Li, A. W. Peters, A. E. Platero-Prats, J. Liu, C. W. Kung, H. Noh, M. R. DeStefano, N. M. Schweitzer, K. W. Chapman, J. T. Hupp, O. K. Farha, *J. Am. Chem. Soc.* 2017, **139**, 15251-15258.
42. A. E. Platero-Prats, A. Mavrandonakis, J. Liu, Z. Chen, Z. Chen, Z. Li, A. A. Yakovenko, L. C. Gallington, J. T. Hupp, O. K. Farha, C. J. Cramer, K. W. Chapman, *J. Am. Chem. Soc.* 2021, **143**, 20090-20094.
43. J. Liu, Z. Chen, R. Wang, S. Alayoglu, T. Islamoglu, S. J. Lee, T. R. Sheridan, H. Chen, R. Q. Snurr, O. K. Farha, J. T. Hupp, *ACS Appl. Mater. Interfaces* 2021, **13**, 22485-22494.
44. D. Yang, M. A. Ortuno, V. Bernales, C. J. Cramer, L. Gagliardi, B. C. Gates, *J. Am. Chem. Soc.* 2018, **140**, 3751-3759.
45. N. Ko, P. G. Choi, J. Hong, M. Yeo, S. Sung, K. E. Cordova, H. J. Park, J. K. Yang, J. Kim, *J. Mater. Chem. A* 2015, **3**, 2057-2064.
46. Z. Wang, K. M. Schmalbach, R. L. Combs, Y. Chen, R. L. Penn, N. A. Mara, A. Stein, *ACS Appl. Mater. Interfaces* 2020, **12**, 49971-49981.

47. A. U. Ortiz, A. Boutin, A. H. Fuchs, Francois-Xavier Coudert, *J. Chem. Phys.* 2013, **138**, 174703.
48. R. Anderson, D. A. Gomez-Gualdron, *Chem. Mater.* 2020, **32**, 8106-8119.
49. J. E. Mondloch, M. J. Katz, W. C. Isley, P. Ghosh, P. Liao, W. Bury, G. W. Wagner, M. G. Hall, J. B. DeCoste, G. W. Peterson, R. Q. Snurr, C. J. Cramer, J. T. Hupp, O. K. Farha, *Nat. Mater.* 2015, **14**, 512-516.
50. Y. Liu, A. J. Howarth, N. A. Vermeulen, S. Y. Moon, J. T. Hupp, O. K. Farha, *Coord. Chem. Rev.* 2017, **346**, 101-111.

 This journal is © The Royal Society of Chemistry 20xx

Please do not adjust margins